To appear in AEGIS Special Issue of ApJ Letters

AEGIS20: a radio survey of the Extended Groth Strip

R. J. Ivison,[1] S. C. Chapman,[2] S. M. Faber,[3] Ian Smail,[4] A. D. Biggs,[1] C. J. Conselice,[5] G. Wilson,[6] S. Salim,[7] J.-S. Huang[8] & S. P. Willner[8]

ABSTRACT

We describe AEGIS20 – a radio survey of the Extended Groth Strip (EGS) conducted with the Very Large Array (VLA) at 1.4 GHz. The resulting catalog contains 1,123 emitters and is sensitive to ultraluminous ($10^{12}\,L_\odot$) starbursts to $z \leq 1.3$, well matched to the redshift range of the DEEP2 spectroscopic survey in this region. We use stacking techniques to explore the μJy-level emission from a variety of galaxy populations selected via conventional criteria – Lyman-break galaxies (LBGs), distant red galaxies (DRGs), UV-selected galaxies and extremely red objects (EROs) – determining their properties as a function of color, magnitude and redshift and their extinction-free contributions to the history of star formation. We confirm the familiar pattern that the star-formation-rate (SFR) density, $\rho_\star$, rises by *at least* $\sim$5$\times$ from $z = 0$ to 1, though we note highly discrepant UV- and radio-based SFR estimates. Our radio-based SFRs become more difficult to interpret at $z > 1$ where correcting for contamination by radio-loud active galactic nuclei (AGN) comes at the price of rejecting luminous starbursts. Whilst stacking radio images is a useful technique, accurate radio-based SFRs for $z \gg 1$ galaxies require precise redshifts and extraordinarily high-fidelity radio data to identify and remove accretion-related emission.

Subject headings: cosmology: observations — galaxies: evolution

[1]UK Astronomy Technology Centre, Royal Observatory, Blackford Hill, Edinburgh EH9 3HJ, UK

[2]Astronomy Department, California Institute of Technology, Pasadena, CA 91125

[3]Department of Astronomy and Astrophysics, University of California, Santa Cruz, Santa Cruz, CA 95064

[4]Institute for Computational Cosmology, Durham University, South Road, Durham DH1 3LE, UK

[5]Physics and Astronomy, University of Nottingham, University Park, Nottingham NG7 2RD, UK

[6]Spitzer Science Center, California Institute of Technology, 1200 E. California Bvd, Pasadena, CA 91125

[7]Department of Physics and Astronomy, University of California, Los Angeles, CA 90095

[8]Harvard-Smithsonian Center for Astrophysics, 60 Garden Street, Cambridge, MA 02138

1. Introduction

The tight correlation between radio and far-IR emission for star-forming galaxies (Helou et al. 1985; Garrett 2002; Kovacs et al. 2006), allows us to push dust-independent surveys down to lower SFRs than is possible in the confusion-limited far-IR/submm wavebands. Moreover, the high mapping speed of facilities such as the Giant Metre-wave Radio Telescope means we can quickly obtain the large samples of faint sources needed for reliable analyses.

The bulk of the far-IR background seen by *COBE* (Fixsen et al. 1998) most likely arises from a large population of luminous and ultraluminous IR galaxies (LIRGs and ULIRGs), their energy originating from dust-obscured star formation and accretion. Individually less luminous than submm galaxies, with $L_{\rm bol} \sim 3 \times 10^{11}\,{\rm L}_{\odot}$, these galaxies are believed to be sufficiently numerous to dominate $\rho_{\star}$ at $z \sim 1$ (Dole et al. 2006).

In this letter we present a new panoramic radio survey – AEGIS20 – undertaken with the National Radio Astronomy Observatory's[9] VLA as part of the All-wavelength Extended Groth Strip International Survey (AEGIS; Davis et al. 2006). AEGIS20 was tuned to detect ULIRGs robustly at $z \sim 1$, with a noise level of $10\,\mu{\rm Jy\,beam^{-1}}$ at 1.4 GHz (cf. Hopkins et al. 2003; Bondi et al. 2003). The resulting catalog, available electronically, contains $\sim 10^3$ faint radio sources – an order of magnitude more than the 5-GHz survey of this region by Fomalont et al. (1991); nearly half are expected to have optical spectra provided by the DEEP2 survey, many with redshifts, as well as photometry across a wide range of wavelengths.

The future goal of AEGIS20 is to measure the 1.4-GHz luminosity function, track the evolution of SFRs in LIRGs and ULIRGs and, using a measure of the local galaxy density of each radio source, study the history of star formation as a function of environment. Here, we present the AEGIS20 catalog and utilise the radio image to estimate SFRs for a number of independent and overlapping galaxy populations selected via conventional criteria.

2. Observations and data reduction

Data were obtained at 1.4 GHz during 2003–05 with the VLA in its B configuration, acquiring seven 3.125-MHz channels every 5 s in each of four IFs. We obtained data in six positions, spaced by $15'$ (see Davis et al. 2006), concentrating in the northern half of the EGS because of the proximity of 3C 295 ($S_{1.4{\rm GHz}} = 23$ Jy). Around 18 hr of data were acquired for

[9]The National Radio Astronomy Observatory is operated by Associated Universities Inc., under a cooperative agreement with the National Science Foundation.

each of the field positions, cycling through them between scans of 1400+621 and 1419+543 to monitor bandpass, amplitude and phase. Absolute flux calibration was set using 3C 286.

Calibrated visibilities and associated weights were used to generate mosaics of $37 \times 512^2 \times 0.8''^2$-pixel images to quilt the VLA's primary beam in each EGS field position. CLEAN boxes were placed tightly around all sources and a series of IMAGR and CALIB tasks were run, clipping the *uv* data after subtracting CLEAN components generated by the third iteration of IMAGR. The central images from each of the pointings were then knitted together using FLATN, ignoring data beyond the primary beam's half-power point, to produce a large mosaic. The synthesized beam is circular, with a FWHM of $\sim$3.8″.

3. Sample definition

To define a sample of radio sources we searched signal-to-noise (S/N) images using the SAD detection algorithm, emulating the technique described by Biggs & Ivison (2006). Sources with $\geq 4\sigma$ peaks were fitted with 2-D Gaussians using JMFIT, those with $\geq 5\sigma$ peaks surviving to be fitted in total intensity. Sources with sizes equal to or smaller than the restoring beam were considered unresolved; their size was constrained to that of the beam. We make no correction for bandwidth smearing in the catalog: this is a small effect ($\sim$5%) given our mosaicing strategy and the use of B configuration. We detect 38, 79, 171, 496 and 1,123 sources with $S_{1.4\mathrm{GHz}} \geq 2,000$, $\geq$800, $\geq$320, $\geq$130 and $\geq 50\,\mu$Jy (consistent with Simpson et al. 2006), where the 5σ detection limits at 130 and 50 μJy cover 0.73 and 0.04 deg^2. Confusion is not an issue: the source density on an arcmin^2 scale is <0.01 beam^{-1}.

$S_{1.4\mathrm{GHz}} = 50\,\mu$Jy corresponds to rest-frame 1.4-GHz luminosities, $L_{1.4\mathrm{GHz}}$, of 0.44, 2.3, 6.0 and 12 $\times 10^{23}$ W Hz^{-1} and SFRs of 50, 275, 725 and 1,430 $\mathrm{M}_\odot\,\mathrm{yr}^{-1}$ at $z = 0.5$, 1.0, 1.5 and 2.0 (for $\Omega_m = 0.27, \Omega_\Lambda = 0.73$, $H_0 = 71\,\mathrm{km\,s^{-1}\,Mpc^{-1}}$ — Spergel et al. 2003 — a Salpeter initial mass function [IMF] with $\mathrm{d}N/\mathrm{d}M \propto M^{-2.35}$ over 0.1–100 $\mathrm{M}_\odot$ and $S_\nu \propto \nu^{-0.8}$).

AEGIS20 covers 57% of the existing DEEP2 region (Davis et al. 2006), with $\sim$7,900 unique redshifts available in the 0.28 deg^2 common to both surveys. DEEP2 thus covers 35% of AEGIS20, although its *BRI* imaging covers 90% of AEGIS20 (93% of cataloged sources). Of the AEGIS20 sources with optical imaging, $\sim$36% have $R_{\mathrm{AB}} < 24.1$ counterparts within 1″. Since the DEEP2 targeting rate is $\sim$70%, the inclusion rate on DEEP2 masks for faint radio emitters is $\sim$25%. At present, $\sim$100 of the targeted AEGIS20 radio sources have DEEP2 redshifts — a very high success rate. Radio properties of DEEP2 galaxies and the spectroscopic properties of the AEGIS20 catalog will be discussed in a forthcoming paper.

4. The radio properties of distant galaxy populations

The wealth of multi-frequency data in AEGIS allows us to mimic the selection of galaxy populations such as DRGs ($J - K > 2.3$; expected to lie at $1.9 < z < 3.5$ — Franx et al. 2003), as well as LBGs (Steidel et al. 2003) and EROs. We investigate the radio properties of several such populations in this section, taking them roughly in order of increasing redshift.

We expect to detect only a small fraction of distant galaxies at radio frequencies. In such situations it is common to assess the emission from a galaxy population using a stacking analysis, accomplished either by extracting and co-adding postage stamps centered on the galaxies of interest ('image stacking') or by co-adding flux densities measured at the positions of the galaxies ('pixel stacking'). We adopt both approaches here. To determine the signal lost by pixel stacking we employed radio emitters with S/N = 5–20 pixel^{-1}, finding a difference of only 3.9% between the values returned at the positions of the emitters and cataloged AEGIS20 flux densities. Monte-Carlo simulations show that the mean $S_{1.4\mathrm{GHz}}$ determined by pixel stacking are slightly skewed ($+0.1\,\mu$Jy, typically) but are otherwise well described by Gaussian statistics; medians are affected at the <0.01-μJy level. $S_{1.4\mathrm{GHz}}$ values have been corrected for bandwidth smearing (+5.0%), for pixel-stacking losses (+3.9%) and we have excluded galaxies in noisy regions ($\sigma_{1.4\mathrm{GHz}} > 30\,\mu\mathrm{Jy\,beam}^{-1}$).

We must excise emission due to accretion if we are to determine accurate radio-based SFRs. Morphological classification of most radio emitters is not feasible at the resolution of our data, spectral indices are not to hand and the availability and reliability of AGN indicators at shorter wavelengths differs widely across the EGS. Radio-loud AGN were thus identified and rejected via a $L_{1.4\mathrm{GHz}}$ limit. Following Condon (1992), we adopt $L_{1.4\mathrm{GHz}} < 10^{24}\,\mathrm{W\,Hz}^{-1}$ for normal galaxies, an order of magnitude below the break in morphology and luminosity noted by Fanaroff & Riley (1974). We quote the noise-weighted mean $S_{1.4\mathrm{GHz}}$; where AGN contamination is extreme (>5%), we quote the median, noting the number of obvious AGN. One unfortunate consequence of excising radio-loud AGN on the basis of $L_{1.4\mathrm{GHz}}$ is the exclusion of distant hyperluminous starbursts lying on the far-IR/radio correlation (§5).

We begin with a ultraviolet (UV)-selected catalog containing 4,426 galaxies detected at 230 nm by *GALEX*, with DEEP2 redshifts, i.e. $R_{\mathrm{AB}} < 24.1$, excluding objects with AGN flags (Salim et al. 2006). Of these, 3,908 lie within the $0.28\,\mathrm{deg}^2$ of common areal coverage with AEGIS20. We compare SFRs determined in two ways – via their UV and radio properties, $\mathrm{SFR_{UV}}$ and $\mathrm{SFR_{rad}}$ – for the same galaxies. We use UV-based, extinction-corrected SFRs, derived by comparing observed spectral energy distributions (SEDs) with those of model galaxies exhibiting a wide range of properties and SF histories (Salim et al. 2005). Appropriate volume corrections for the *GALEX*-selected sample are difficult to determine

due to a complex selection function dependent on UV/optical magnitudes and spectral characteristics. We therefore correct for the rate with which *GALEX* detects DEEP2 galaxies, which is known to fall from 90–75–60% at $z = 0.2$–1.0–1.4, but not for our steadily decreasing sensitivity to low-luminosity galaxies (Arnouts et al. 2005). Because of this, we are limited to discussing the ratio of $\rho_{\star(\mathrm{UV})}$ and $\rho_{\star(\mathrm{rad})}$ within the sample.

Robust radio detections of the UV sample were possible by pixel stacking over $\Delta z = 0.2$ bins. Only 11 radio-loud AGN were identified via $L_{1.4\mathrm{GHz}}$, $<<1\%$ of the total; having rejected these, noise-weighted means provide the most appropriate measure of SFR for this sample (Table 1). $\mathrm{SFR_{UV}}$ and $\mathrm{SFR_{rad}}$ per UV-selected galaxy both increase with redshift, unsurprisingly since we are probing more UV-luminous galaxies at larger distances. For $z = 0$–1, $\rho_{\star(\mathrm{UV})}$ remains fairly constant whilst $\rho_{\star(\mathrm{rad})}$ rises rapidly. It may seem puzzling that $\rho_{\star(\mathrm{UV})}$ at $z \sim 0$ is an order of magnitude higher than $\rho_{\star(\mathrm{rad})}$ (Fig. 1) — $\rho_{\star(\mathrm{rad})}$ should be sensitive to all recent star formation, obscured and unobscured, for a constant IMF — however, Bell (2003) showed that $L_{\mathrm{far-IR}}/L_{\mathrm{UV}}$ varies by $\gtrsim 30\times$ between 0.01 and $3\,\mathrm{L}_\star$ and that radio data underestimate SFRs in low-luminosity galaxies typical of those detected locally by *GALEX*. Hopkins & Beacom (2006) argue that for the full picture we should add $\mathrm{SFR_{UV}}$ and $\mathrm{SFR_{rad}}$. $\rho_{\star(\mathrm{rad})}$ and $\rho_{\star(\mathrm{UV})}$ achieve parity at $z \sim 0.4$, after which $\rho_{\star(\mathrm{rad})}$ continues to rise until $z \sim 0.7$ (cf. Cowie et al. 2004) when incompleteness seriously impacts the sample. Although it is tempting to speculate that the rise in $\rho_{\star(\mathrm{rad})}$ results from the increasing dominance of dust-obscured IR-luminous galaxies, we must recall our sample's origins. We are witnessing an increasing SFR per *UV-selected* galaxy, partly because at $z \sim 1$ we are probing the most UV-luminous galaxies; we are also witnessing an increase in $\rho_{\star(\mathrm{rad})}$ *despite* the increasing incompleteness. Adding $\mathrm{SFR_{UV}}$ and $\mathrm{SFR_{rad}}$, $\rho_\star$ due to UV-selected galaxies increases as *at least* $(1+z)^{2.2}$ between $z = 0$ and 1 (cf. Schiminovich et al. 2005).

The mismatch between the absolute and relative rates of SF derived using UV- and radio-based indicators is worrying, particularly the difference between local estimates of $\rho_\star$. The local $\rho_{\star(\mathrm{UV})}$ matches the $\rho_\star$ compilation presented by Hopkins & Beacom (2006), which implies the UV-selected sample accounts for most of the SF in the local Universe, yet the UV sample at $0.0 < z < 0.2$ accounts for $\ll 1\%$ of the total cataloged $S_{1.4\mathrm{GHz}}$ in the region of common areal coverage. If the fraction of $S_{1.4\mathrm{GHz}}$ due to obscured SF at $0.0 < z < 0.2$ exceeds 1%, $\rho_\star$ would then be at the upper envelope of commonly accepted values.

Moving to slightly higher redshifts, we take two catalogs of EROs. One uses the conventional color cut $R - K_\mathrm{s} > 5.3$ with $K_\mathrm{s} < 20.5$ and DEEP2 redshifts, $1.0 < z < 1.5$ (Conselice et al., in prep). It contains 382 objects in low-noise areas of our radio image. The second (Wilson et al. 2006) uses $R_{\mathrm{AB}} - 3.6\mu\mathrm{m} > 4$ to select essentially the same class of objects, but the larger area covered at $3.6\,\mu$m (and no requirement for redshifts) yields 2,363 objects

in $0.26\,\mathrm{deg}^2$ of AEGIS20. We assumed $z = 1.1$ to excise radio-loud AGN from this sample.

Both ERO samples are well detected at 1.4 GHz, as shown in Fig. 2. In the spectroscopic sample, mean $S_{1.4\mathrm{GHz}}$ does not vary significantly as a function of color, though it is a function of K_s consistent with the findings of Smail et al. (2002). Median $L_{1.4\mathrm{GHz}}$ is $8.1 \times 10^{22}\,\mathrm{W\,Hz^{-1}}$ and the median SFR per ERO is $92 \pm 7\,\mathrm{M_\odot\,yr^{-1}}$. In the sample volume set by the redshift limits and survey area this equates to $\rho_\star = 0.07\,\mathrm{M_\odot\,yr^{-1}\,Mpc^{-3}}$ (cf. Georgakakis et al. 2006; Simpson et al., in prep).

The larger ERO sample reveals a weak trend for $S_{1.4\mathrm{GHz}}$ to increase with redness; this is confirmed by the increasing detection rate for individual objects (Table 1). Mean $S_{1.4\mathrm{GHz}}$ also declines as $S_{3.6\mu\mathrm{m}}$ decreases. We expect $S_{3.6\mu\mathrm{m}}$ to trace stellar mass and distance, and the factor of $\sim$5.5 decrease in $S_{1.4\mathrm{GHz}}$ for a for a factor of $\sim$15 decrease in $S_{3.6\mu\mathrm{m}}$ suggests an increasing SFR per unit stellar mass as redshift increases. The overall $\rho_\star$ for this sample is consistent with that of the spectroscopic sample, as expected given the limited number of spectroscopic redshifts and the significant sample overlap.

Huang et al. (in prep) present a catalog selected at $S_{24\mu\mathrm{m}} > 150\mu$Jy, with $S_{4.5\mu\mathrm{m}} > S_{3.6\mu\mathrm{m}}$, aiming to select galaxies and AGN at $z > 1.5$. Almost 10^3 objects lie in low-noise regions of our radio mosaic, overlapping AEGIS20 by $0.26\,\mathrm{deg}^2$. The individual radio detection rate is a strong function of $S_{24\mu\mathrm{m}}$, rising from 30 to 70% between $S_{24\mu\mathrm{m}} = 0.15$ and >1.2 mJy. Median $S_{1.4\mathrm{GHz}}$ (Table 1) is fairly insensitive to R_AB, varying by $<2\times$ over >3 mag. Over 40% of the 24-μm-selected galaxies have $L_{1.4\mathrm{GHz}} > 10^{24}\,\mathrm{W\,Hz^{-1}}$ when assuming $z = 2.75$. At this redshift *all* S/N ≥ 3 measurements imply radio-loud AGN and it is difficult to estimate the SFR: $\rho_\star$ is likely to be high, but so is the level of accretion-related contamination. The median $S_{1.4\mathrm{GHz}}$, $28\,\mu$Jy, translates into $\rho_\star = 0.20\,\mathrm{M_\odot\,yr^{-1}\,Mpc^{-3}}$ for $z = 1.5$–4. We would be unsurprised if this is in error by $\times 2$; regardless, this is an important star-forming population.

Moving on to yet more distant populations, this time to a sample of DRGs selected at $K_\mathrm{s} < 20.5$ (Vega) with $J - K_\mathrm{s} > 2.3$ (Conselice et al. 2006), 108 of which lie within the $0.11\,\mathrm{deg}^2$ of common coverage with AEGIS20. Although expected to lie at $1.9 < z < 3.5$ (Franx et al. 2003), Conselice et al. find that 64% lie at $1 < z < 2$. Galaxies with $z < 1$, evident via DEEP2, have been removed from the sample used here. One of the radio emitting DRGs has $L_{1.4\mathrm{GHz}}$ consistent with radio-loud AGN (or, as noted earlier, a hyperluminous starburst). The mean $S_{1.4\mathrm{GHz}}$ for the DRGs was $10.1 \pm 1.3\,\mu$Jy – faint emission can be seen in the stacked S/N image (Fig. 2). At $z = 1.5$ this corresponds to $L_{1.4\mathrm{GHz}} = (1.2 \pm 0.2) \times 10^{23}\,\mathrm{W\,Hz^{-1}}$ and a mean SFR (per DRG) of $150 \pm 19\,\mathrm{M_\odot\,yr^{-1}}$. Knudsen et al. (2005) found $190 \pm 50\,\mathrm{M_\odot\,yr^{-1}}$ using submm data for a sample of 30 DRGs (adapting to the cosmology and IMF used here), having assumed significantly larger distances. The observed radio emission from $K_\mathrm{s} < 20.5$ DRGs equates to $\rho_\star = 0.02\,\mathrm{M_\odot\,yr^{-1}\,Mpc^{-3}}$ at $z = 1$–2.

The LBGs of Steidel et al. (2003) lie in a noisy region of the radio mosaic. Of the 334 cataloged LBGs, after correction for the astrometric offset in that catalog ($\Delta\alpha = +0.8''$, $\Delta\delta = +2.6''$), 107 lie within low-noise regions of the radio mosaic; their mean $S_{1.4\mathrm{GHz}}$ was $2.0 \pm 2.3\,\mu$Jy (median, $-0.6\,\mu$Jy), consistent with an average SFR of $<500\,\mathrm{M}_\odot\,\mathrm{yr}^{-1}$ ($3\,\sigma$, for $z = 3$). Restricting the catalog to the 53 LBGs detected at $8\,\mu$m with IRAC did not change the situation significantly (cf. Rigopoulou et al. 2006).

Finally, Huang et al. (2005) describe a population of IR-luminous LBGs (ILLBGs) detected at $S_{24\mu\mathrm{m}} > 60\mu$Jy. Only six of Huang et al.'s 13 objects lie within our radio mosaic. Their median $S_{1.4\mathrm{GHz}}$ is $44.2\,\mu$Jy, including the one significant detection: Westphal MD99 at $\sim$1 mJy. This provides tentative support for the assertion that ILLBGs share the high SFRs of submm galaxies, though this is a very small sample in a particularly noisy region of the radio mosaic and accretion-related contamination is possible. If, as Huang et al. suggest, ILLBGs lie at $2 < z < 3$ (like submm galaxies – Chapman et al. 2005) then their $\rho_\star$ is similar to that of the 24μm-selected galaxies with which they will overlap significantly (Fig. 1).

5. On radio data as a probe of global SF history

Fig. 1 shows $\rho_\star$ for the galaxy populations explored in §4. The upper envelope of points traces the minimum $\rho_\star$ as a function of redshift and appears to rise by at least $5\times$ from $z = 0$ to 1, a now-familiar pattern (Lilly et al. 1996), though this work has led us to question the reliability of many SFR and $\rho_\star$ estimates.

Radio-based SFR estimates become increasingly prone to contamination by radio-loud AGN at $z \gg 1$. Unfortunately, a consequence of removing this via a limit on $L_{1.4\mathrm{GHz}}$ is the rejection of luminous star-forming galaxies obeying the far-IR/radio correlation; adopting a median $S_{1.4\mathrm{GHz}}$ is unlikely to be better. In addition, some redshift-limited galaxy populations defined by color appear less well defined than first claimed (Conselice et al. 2006), limiting our ability to judge the volume probed. These effects lead to large uncertainties so while it is clear that stacking radio data is useful, accurate SFRs for distant galaxies require precise redshifts together with deep, multi-frequency, high-resolution radio data ($\ll 1''$, $\sigma_{0.6\mathrm{GHz}} \sim \sigma_{1.4\mathrm{GHz}} \lesssim 1\,\mu$Jy). These will facilitate identification and removal of accretion-related emission via radio luminosity, spectral index, brightness temperature and morphology.

REFERENCES

Arnouts, S., et al. 2005, ApJ, 619, L43

Bell, E.F. 2003, ApJ, 586, 794

Biggs, A.D., & Ivison, R.J. 2006, MNRAS, 371, 963

Bondi, M., et al. 2003, A&A, 403, 857

Chapman, S.C., Blain, A.W., Smail, I., & Ivison, R.J. 2005, ApJ, 622, 772

Condon, J.J. 1992, ARA&A, 315, 575

Conselice, S.C., et al. 2006, ApJ, in press (this issue)

Cowie, L.L., Barger, A.J., Fomalont, E.B., & Capak, P. 2004, ApJ, 603, L69

Davis, M., et al. 2006, ApJ, in press (this issue)

Dole, H., et al. 2006, A&A, 451, 417

Fanaroff, B.L., & Riley, J.M. 1974, MNRAS, 167, 31

Fixsen, D.J., Dwek, E., Mather, J.C., Bennett, C.L., & Shafer, R.A. 1998, ApJ, 508, 123

Fomalont, E.B., Windhorst, R.A., Kristian, J.A., & Kellerman, K.I. 1991, AJ, 102, 1258

Franx, M., et al. 2003, ApJ, 587, L79

Garrett, M.A. 2002, A&A, 384, L19

Georgakakis, A., Hopkins, A.M., Afonso, J., Sullivan, M., Mobasher, B., & Cram, L.E. 2006, MNRAS, 367, 331

Helou, G., Soifer, B.T., & Rowan-Robinson, M. 1985, ApJ, 298, L7

Hopkins, A.M., Afonso, J., Chan, B., Cram, L.E., Georgakakis, A., & Mobasher, B. 2003, AJ, 125, 465

Hopkins, A.M., & Beacom, J.F. 2006, ApJ, in press (astro-ph/0601463)

Huang, J.-S., et al. 2005, ApJ, 634, 137

Knudsen, K.K., et al. 2005, ApJ, 632, L9

Kovács, A., Chapman, S.C., Dowell, C.D., Blain, A.W., Ivison, R.J., Smail, I., & Phillips, T.G. 2006, ApJ, in press (astro-ph/0604591)

Lilly, S.J., Le Fevre, O., Hammer, F., & Crampton, D., 1996, ApJ, 460, L1

Rigopoulou, D., et al. 2006, ApJ, 648, 81

Salim, S., et al. 2005, ApJ, 619, L39

Salim, S., et al. 2006, ApJ, in press (this issue)

Schiminovich, D., et al. 2005, ApJ, 619, L47

Simpson, C., Rawlings, S., Martínez Sansigre, A., Ivison, R.J., Sekiguchi, K., & Takata, T. 2006, MNRAS, in press (astro-ph/0609529)

Smail, I., Owen, F.N., Morrison, G.E., Keel, W.C., Ivison, R.J., & Ledlow, M.J. 2002, ApJ, 581, 844

Spergel, D.N., et al. 2003, ApJS, 148, 175

Steidel, C.C., Adelberger, K.L., Shapley, A.E., Pettini, M., Dickinson, M., & Giavalisco, M. 2003, ApJ, 592, 728

Wilson G., et al. 2006, ApJ, in press (this issue)

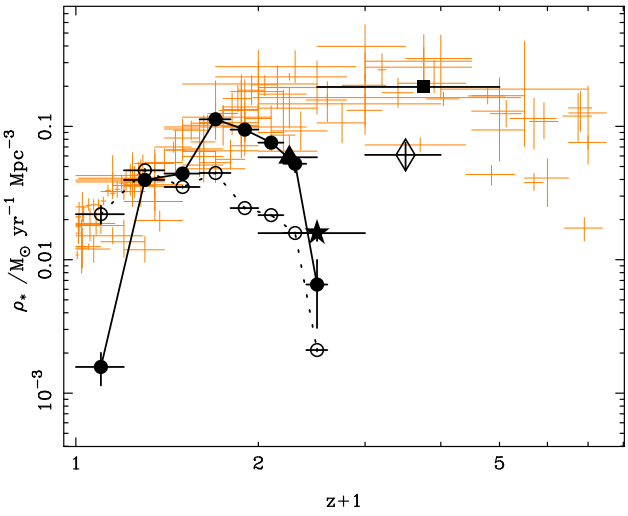

Fig. 1.— Radio-based estimates of SFR density ($\rho_\star$) for a number of independent and overlapping galaxy populations selected via magnitude and color criteria: UV-selected galaxies (open and filled circles for UV- and radio-based SFRs, joined by dotted and solid lines), $R - K_s > 5.3$ EROs (triangle), DRGs (star), ILLBGs (diamond) and 24-μm-selected galaxies (filled square). These are conservative estimates – no attempt has been made to correct for accessible volume; contamination by radio-loud AGN is possible at $z \gg 1$ (§5). The upper envelope of points thus traces the minimum $\rho_\star$ as a function of redshift, as demonstrated by the compilation of $\rho_\star$ data from Hopkins & Beacom (2006), plotted faintly here.

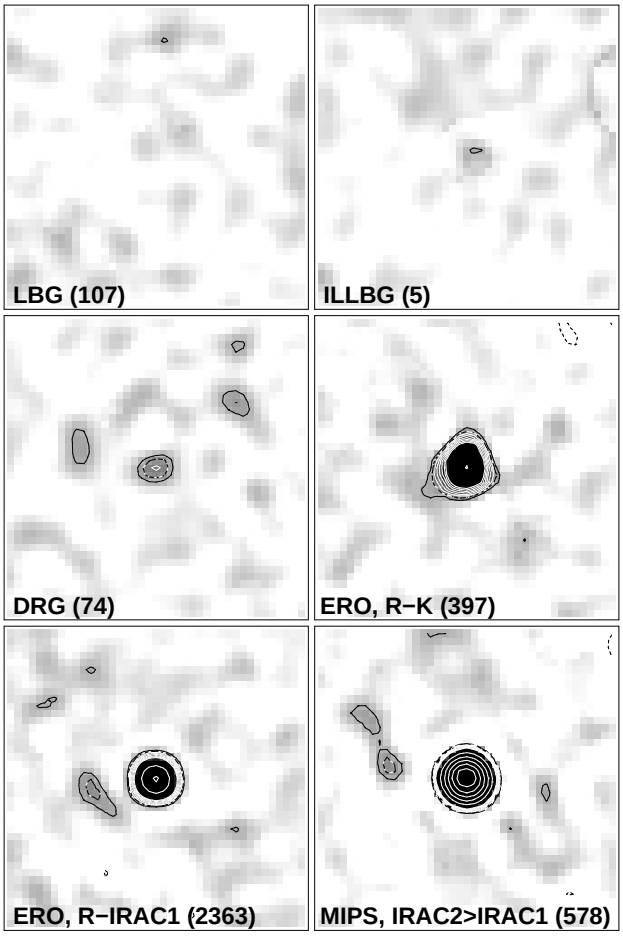

Fig. 2.— Stacked S/N images ($33'' \times 33''$) at the positions of the galaxies described in §4: conventional and IR-luminous LBGs (top row); DRGs and $R - K_{\rm s} > 5.3$ EROs (middle row); IRAC-selected EROs and MIPS-selected galaxies with $S_{4.5\mu{\rm m}} > S_{3.6\mu{\rm m}}$ (bottom row). Areas of high noise and galaxies detected individually ($\geq 5\sigma$) were excluded. Contours are plotted at S/N levels of $-3, 3, 4...10, 20...100$ and the greyscale is identical in each case. The number of stacked sources from each population is shown in parentheses. The detection of the IRAC-selected ERO population is so significant that we see secondary structure: the image resembles the dirty beam since none of the individually undetected sources in the ensemble that makes up the stacked image have been CLEANed.

Table 1. SINGLE-COLUMN: 1.4-GHz flux densities ($S_{1.4\mathrm{GHz}}$, in μJy) and SFRs determined by pixel stacking at the positions of galaxies in the samples discussed in §4

Sample[a] (§4)	Selection criteria	N[b]	$S_{1.4\mathrm{GHz}}$	SFR[c]
UV-selected	z=0.0–0.2	136-0-0	4.1±1.1	0.12
galaxies,	z=0.2–0.4	678-9-0	11.2±0.5	3.6
R_{AB}<24.1	z=0.4–0.6	612-12-1	8.4±0.5	8.9
	z=0.6–0.8	1,055-20-2	8.8±0.4	21
	z=0.8–1.0	667-7-0	8.5±0.5	36
	z=1.0–1.2	441-7-5	6.8±0.6	47
	z=1.2–1.4	276-3-2	5.7±0.8	59
	z=1.4–1.6	30-1-1	4.5±2.4	65
EROs,	R–K_{s}=5.3–5.6	216-14-7	13.6±0.8	126
K_{s}<20.5	R–K_{s}>5.6	170-15-8	11.9±0.9	111
R–K_{s}>5.3	K_{s}=17–18	35-7-4	20.6±2.2	194
	K_{s}=18–19	187-19-10	16.9±0.9	159
	K_{s}=19–20	140-3-1	6.3±1.0	59
	K_{s}=20–21	19-0-0	12.9±2.8	121
EROs,	R_{AB}–3.6=4.0–4.5	1,027-53-17	11.8±0.4	81
R_{AB}–3.6>4	R_{AB}–3.6=4.5–5.0	720-29-4	10.6±0.4	73
	R_{AB}–3.6=5.0–5.5	437-29-8	14.4±0.6	100
	R_{AB}–3.6=5.5–6.0	137-11-2	16.7±1.0	115
	R_{AB}–3.6>6.0	42-8-1	27.7±1.8	192
	3.6μm=19–20	411-62-15	25.1±0.6	174
	3.6μm=20–21	1032-48-9	13.1±0.4	90
	3.6μm=21–22	742-10-1	6.4±0.4	44
	3.6μm>22	154-3-2	4.6±0.9	32
24μm	S_{24}=0.15–0.3 mJy	634-65-291	23.5	1,400
galaxies,	S_{24}=0.3–0.6 mJy	196-61-89	41.6	2,480
$S_{4.5}$>$S_{3.6}$	S_{24}=0.6–1.2 mJy	67-34-21	67.2	4,010
	S_{24}>1.2 mJy	29-19-2	103	6,120
	R_{AB}<23	173-46-86	38.0	2,260
	R_{AB}=23–24	154-39-67	32.7	1,950
	R_{AB}=24–25	222-43-87	27.5	1,640
	R_{AB}=25–26	151-26-69	29.0	1,730
	R_{AB}>26	92-7-41	21.7	1,290
DRGs,	K_{s}<20.5	80-2-1	10.1±1.3	150
J–K_{s}>2.3				
LBGs		107-0-28	2.0±2.3	<500
ILLBGs	S_{24}>0.06 mJy	6-1-4	44.2±11.5	2,120

[a]Units are magnitudes unless otherwise stated

[b]Number of sources, number detected individually (S/N $\geq$ 5) and number classified as radio-loud AGN

[c]Radio-based SFR per object; for the R_{AB}–3.6 EROs, we assume $z = 1.1$; for the 24-μm-selected galaxies, we assume $z = 2.75$